Soft X-ray Excesses and X-ray Line Variability in Cygnus X-3

Angelo Varlotta[1,2], Michael McCollough[1,2]

[1,2]Harvard-Smithsonian Center for Astrophysics, Cambridge MA, avarlotta@cfa.harvard.edu, mmccollough@cfa.harvard.edu

Abstract

Cyg X-3 is an X-ray binary (XRB) system containing a stellar-mass compact object, most likely a black hole, and a Wolf-Rayet companion star, which produces collimated, relativistic jets, placing it in the sub-class of XRBs known as microquasars. Cyg X-3 was observed by the Chandra ACIS-S HETG on 2006, January 26 for 50 ks, which corresponds to almost three orbits of Cyg X-3. Our Chandra analyses focused on the line variations and changes in the flux continuum that occur over the orbital phase. The orbital-dependent line features hint to the line-of-sight geometry of the binary system and highlight physical emission effects and changes in the continuum flux. We have also used X-ray data that is part of Swift/RXTE campaign to investigate a soft X-ray excess around 1 KeV (Apr 2010 - Apr 2011), which appears to be similar to the variable soft emission observed in Seyfert galaxies. The presence of the soft X-ray feature in Cyg X-3 would argue for a greater support of the black-hole nature of the compact object and serve to better highlight the similarities of microquasars and AGN. We present the results of our investigations of these orbital-phased features, as well as the variations of the X-ray Fe line region (6.4-7.0 keV) as a function of the state activity and orbital phase.

Introduction

Cyg X-3 has long been considered a puzzling X-ray source. Its 4.8-hour orbital period is characteristic of low-mass X-ray binaries (LMXBs) but infrared spectroscopy has revealed a Wolf-Rayet companion star, making it a high-mass X-ray binary (HMXBs). The strong dense winds from the companion star make it difficult to measure the nature of the compact object (black hole or neutron star). The system is known to undergo spectral state changes in the X-rays (Szostek et al. 2008). In the radio, a relativistic jet has been observed and is closely aligned with our line of sight. An evident link between hard X-ray and radio emission has been detected in Cyg X-3, with the radio and hard X-ray quenching preceding a major radio flare (McCollough et al. 1999). The entrance into the radio-quenching state marks the moment when the source enters the hypersoft state, which may be linked to the GeV emission (Koljonen et al. 2010).

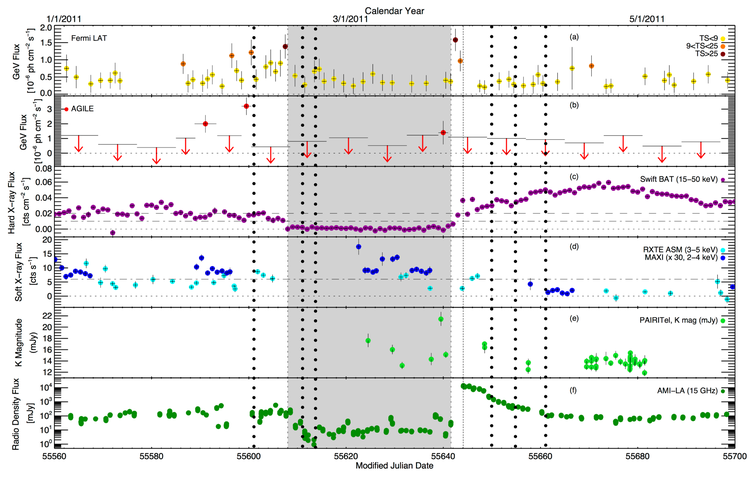

Figure 1: Fermi LAT (0.1-100 GeV, top), AGILE (0.1-3 GeV, second from top), Swift BAT (15-50 keV, third from top), RXTE ASM/MAXI (3-5 keV/ 2-4 keV, third from bottom), PAIRITel (IR K band, second from bottom) and AMI-LA (15 GHz, bottom) light curves. The thick dashed vertical lines display the Swift XRT observations, while the grey area delimits the radio-quenched state (McCollough et al., 2011 HEAD Meeting).

Preliminary Results

The Chandra and Swift fits were accomplished by use of simple spectral models, namely the Xspec models `phabs` (photo-absorption model), `pcfabs` (partially covered absorption model, just used for the Chandra data) and `diskbb` (multi-temperature disk blackbody model). The many line and edge features were fitted with `gabs` (gaussian absorption model), `gau` (gaussian emission model), `edge` (absorption edge model) and `redge` (radiative recombination continua model). The energy range was limited to 1.5 - 7 KeV for the Chandra data, while the Swift data energy range is 1-10 keV.

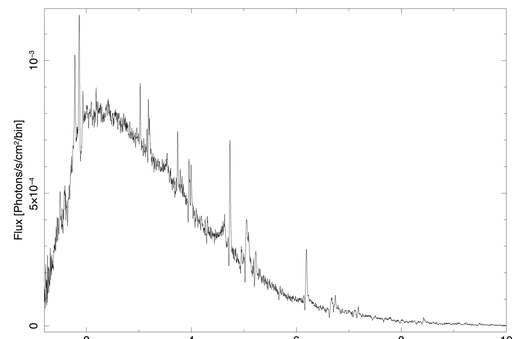

Figure 1: Many are the well known line features visible in this Chandra spectrum of Cyg X-3. Prominent, known spectral features were fitted with a gaussian and/or an absorption edge, with the Xspec models `gau` and/or `gabs`. Conversion factor: 1 Å = 12.398 keV.

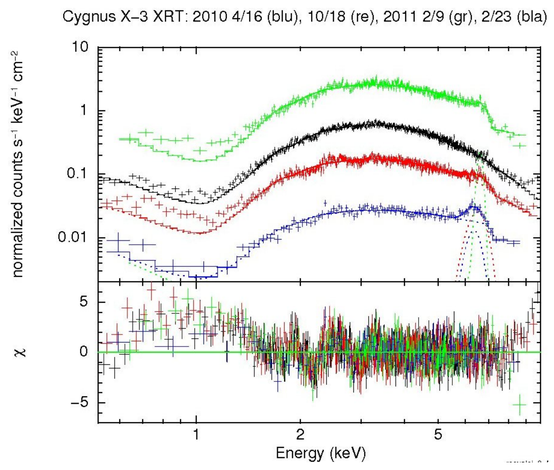

Figure 2: The soft features at the low energy end are visible in this composite Swift XRT spectra of Cyg X-3 (2010-04-16 and 2011-02-09).

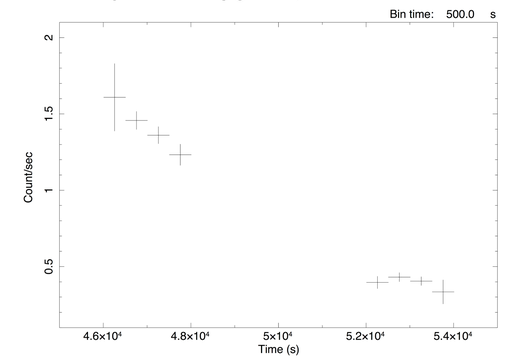

Figure 3: The light curve of the soft excess feature of Cyg X-3, in the 0.5-1.0 keV energy range (MJD 55601, 2011-02-09).

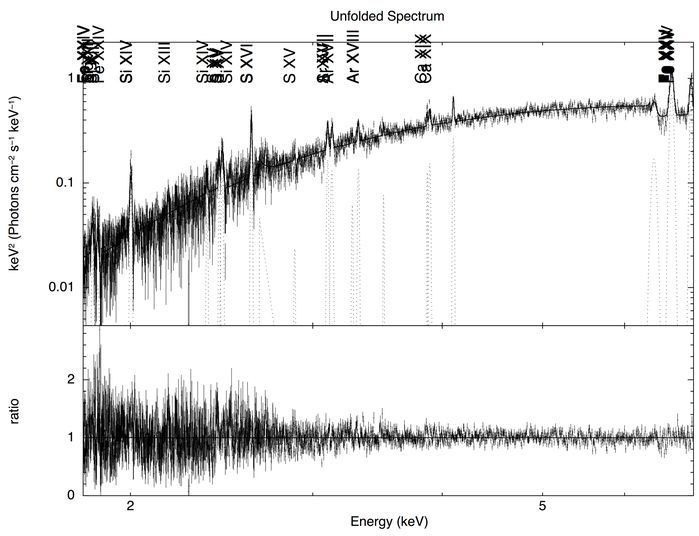

Figure 4: Orbital phase bin: 0.0-0.2. The fits makes use of the Xspec models `phabs`, `pcfabs`, `diskbb`, `gabs`, `gau`, `edge` and `redge`. T_{disk}=2.4 keV, N_h=2.7*10^{22} cm^{-2}, N_{pc}=4.5*10^{22} cm^{-2}, f_{pc}=0.62, *F(1-8 keV)*= 7.6*10^{-10} ergs s^{-1} cm^{-2} and *L(1-8 keV)*=7.4*10^{36} ergs s^{-1}.

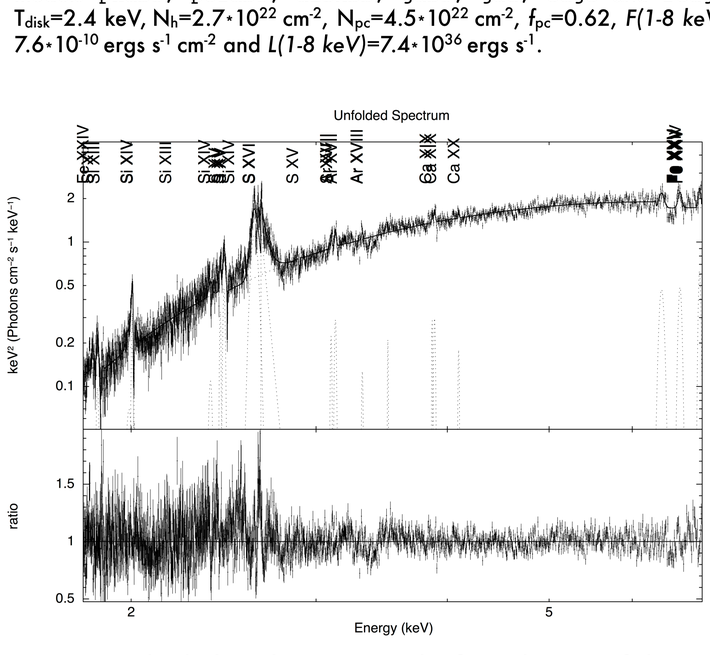

Figure 5: Orbital phase bin: 0.2-0.4. The fits makes use of the Xspec models `phabs`, `pcfabs`, `diskbb`, `gabs`, `gau`, `edge` and `redge`. T_{disk}=2.4 keV, N_h=2.6*10^{22} cm^{-2}, N_{pc}=2.3*10^{22} cm^{-2}, f_{pc}=0.60, *F(1-8 keV)*= 2.9*10^{-9} ergs s^{-1} cm^{-2} and *L(1-8 keV)*=2.8*10^{37} ergs s^{-1}.

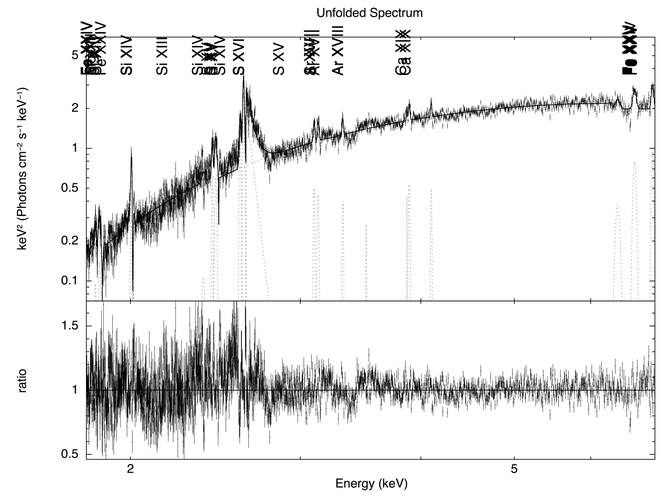

Figure 6: Orbital phase bin: 0.4-0.6. The fits makes use of the Xspec models `phabs`, `pcfabs`, `diskbb`, `gabs`, `gau`, `edge` and `redge`. T_{disk}=2.4 keV, N_h=2.7*10^{22} cm^{-2}, N_{pc}=0.8*10^{22} cm^{-2}, f_{pc}=0.76, *F(1-8 keV)*= 3.4*10^{-9} ergs s^{-1} cm^{-2} and *L(1-8 keV)*=3.3*10^{37} ergs s^{-1}.

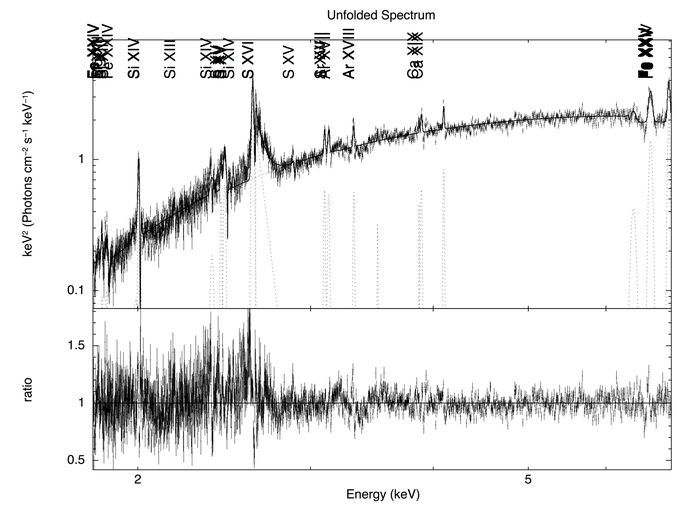

Figure 7: Orbital phase bin: 0.6-0.8. The fits makes use of the Xspec models `phabs`, `pcfabs`, `diskbb`, `gabs`, `gau`, `edge` and `redge`. T_{disk}=2.4 keV, N_h=2.7*10^{22} cm^{-2}, N_{pc}=0.7*10^{22} cm^{-2}, f_{pc}=0.9, *F(1-8 keV)*= 3.4*10^{-9} ergs s^{-1} cm^{-2} and *L(1-8 keV)*=3.3*10^{37} ergs s^{-1}.

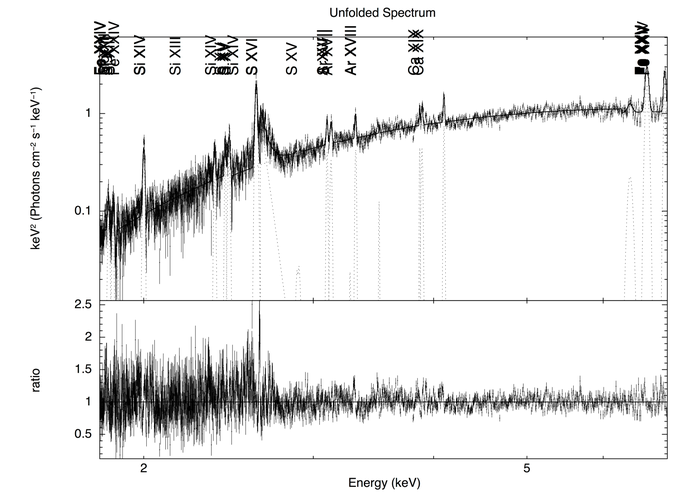

Figure 8: Orbital phase bin: 0.8-1.0. The fits makes use of the Xspec models `phabs`, `pcfabs`, `diskbb`, `gabs`, `gau`, `edge` and `redge`. T_{disk}=2.5 keV, N_h=2.7*10^{22} cm^{-2}, N_{pc}=3.6*10^{22} cm^{-2}, f_{pc}=0.58, *F(1-8 keV)*= 1.7*10^{-9} ergs s^{-1} cm^{-2} and *L(1-8 keV)*=1.6*10^{37} ergs s^{-1}.

Conclusions

Our preliminary results suggest noticeable variations in line emissions and flux variations over the course of the orbital phase. Some of the spectra still present non-optimal residuals at the low energies, which are solved by a partially covering absorption factor (`pcfabs`). Line-of-sight to the observer seems to play a major role in line strength, especially as seen in the S XVI complex (around 2.6 KeV) and close radiative recombination continua, which is noticeable in all orbital phases except for the first phase (0.0-0.2).

Many of these line features outlined here for Cyg X-3 are known emission characteristics of Seyfert galaxies, and confirming these features for Cyg X-3 and other stellar-mass black holes and microquasars (such as Cyg X-1) would be a powerful indicator of the analogy of microquasars and AGN.

Acknowledgements: AV and MLM wish to thank NASA for the financial support through the Fermi Guest Investigator Program.